Electron Transfer in Human Methionine Synthase Reductase Studied by Stopped-Flow Spectrophotometry†

Kirsten R. Wolthers and Nigel S. Scrutton*

Department of Biochemistry, University of Leicester, University Road, Leicester, LE1 7RH, United Kingdom

Received September 10, 2003; Revised Manuscript Received November 14, 2003

ABSTRACT: Human methionine synthase reductase (MSR) is a key enzyme in folate and methionine metabolism as it reactivates the catalytically inert cob(II)alamin form of methionine synthase (MS). Electron transfer from MSR to the cob(II)alamin cofactor coupled with methyl transfer from *S*-adenosyl methionine returns MS to the active methylcob(III)alamin state. MSR contains stoichiometric amounts of FAD and FMN, which shuttle NADPH-derived electrons to the MS cob(II)alamin cofactor. Herein, we have investigated the pre-steady state kinetic behavior of the reductive half-reaction of MSR by anaerobic stopped-flow absorbance and fluorescence spectroscopy. Photodiode array and single-wavelength spectroscopy performed on both full-length MSR and the isolated FAD domain enabled assignment of observed kinetic phases to mechanistic steps in reduction of the flavins. Under single turnover conditions, reduction of the isolated FAD domain by NADPH occurs in two kinetically resolved steps: a rapid (120 s^{-1}) phase, characterized by the formation of a charge-transfer complex between oxidized FAD and NADPH, is followed by a slower (20 s^{-1}) phase involving flavin reduction. These two kinetic phases are also observed for reduction of full-length MSR by NADPH, and are followed by two slower and additional kinetic phases (0.2 and 0.016 s^{-1}) involving electron transfer between FAD and FMN (thus yielding the disemiquinoid form of MSR) and further reduction of MSR by a second molecule of NADPH. The observed rate constants associated with flavin reduction are dependent hyperbolically on NADPH and [4(*R*)-^{2}H]-NADPH concentration, and the observed primary kinetic isotope effect on this step is 2.2 and 1.7 for the isolated FAD domain and full-length MSR, respectively. Both full-length MSR and the separated FAD domain that have been reduced with dithionite catalyze the reduction of $NADP^+$. The observed rate constant of reverse hydride transfer increases hyperbolically with $NADP^+$ concentration with the FAD domain. The stopped-flow kinetic data, in conjunction with the reported redox potentials of the flavin cofactors for MSR [Wolthers, K. R., Basran, J., Munro, A. W., and Scrutton, N. S. (2003) *Biochemistry*, *42*, 3911−3920], are used to define the mechanism of electron transfer for the reductive half-reaction of MSR. Comparisons are made with similar stopped-flow kinetic studies of the structurally related enzymes cytochrome P450 reductase and nitric oxide synthase.

Methionine synthase reductase (MSR[1]; EC 2.1.1.135) is a 78-kDa diflavin enzyme containing one equivalent each of FAD and FMN (*1*). MSR transfers electrons derived from NADPH oxidation through its flavin centers to its physiological redox partner, cobalamin-dependent methionine synthase (MS; *2*). The cob(I)alamin cofactor of MS abstracts a methyl group from methyltetrahydrofolate forming the intermediate methylcob(III)alamin and tetrahydrofolate. The MS catalytic cycle is complete with subsequent methyl transfer from methylcob(III)alamin to homocysteine, forming methionine and cob(I)alamin (*3*). Occasionally, MS is rendered inactive with the aberrant one-electron oxidation of the highly nucleophilic cob(I)alamin form of the cofactor. Electron transfer from MSR and donation of a methyl group from *S*-adenosyl methionine converts cob(II)alamin to methylcob(III)alamin (*4*). MS subsequently returns to the primary turnover cycle as the enzyme is poised to catalytically transfer a methyl group to homocysteine forming methionine.

The role of MSR in reactivating MS makes it a key enzyme in mammalian methionine and folate metabolism, and this is apparent through a number of clinically relevant polymorphisms in the gene encoding MSR. These mutations, which map to the *cbl*E complementation group, lead to an autosomal recessive disorder in which the conversion of homocysteine to methionine is impaired (*5*). Epidemiological studies have shown that elevated plasma homocysteine is a risk factor for coronary arterial disease (*6*, *7*), neural tube defects (*8*, *9*), and Down's syndrome (*10*). These polymorphic variants of MSR potentially have altered kinetic and/or thermodynamic properties that impair the reductive reactivation of MS.

† This work was supported by the Lister Institute of Preventive Medicine, the Wellcome Trust, and by a postdoctoral fellowship from the National Institutes of Health (K.R.W.). N.S.S. is a Lister Institute Research Professor.

* Corresponding author. Telephone: +44 116 223 1337. Fax: +44 116 252 3369. E-mail: nss4@le.ac.uk.

[1] Abbreviations: MSR, methionine synthase reductase; MS, methionine synthase; FNR, ferredoxin-$NADP^+$ oxidoreductase; FLD, flavodoxin; CPR, cytochrome P450 reductase; NOS, nitric oxide synthase; NR1, human novel oxidoreductase 1; ox, oxidized; sq, semiquinone; hq, hydroquinone.

10.1021/bi0356303 CCC: $27.50
Published on Web 12/20/2003

Sequence analysis of MSR (*1*) reveals that it is a member of the family of mammalian diflavin reductases, which includes cytochrome P450 reductase (CPR; *11*), human novel oxidoreductase 1 (NR1; *12*), and the reductase domain of nitric oxide synthase (NOS; *13*). These enzymes have a NADPH/FAD-binding domain, homologous to bacterial ferredoxin $NADP^+$-oxidoreductase (FNR), and a covalently tethered FMN-binding domain that is related to bacterial flavodoxin (FLD). MSR and the other mammalian diflavin reductases may have arisen from the fusion of genes encoding these two bacterial proteins or their progenitors. There is functional evidence for this evolutionary link with MSR since the *Escherichia coli* MS cob(II)alamin cofactor is reductively methylated by a two-component flavoprotein system involving FNR-like protein and FLD (*4*, *14*).

We recently cloned, expressed, and purified MSR in addition to its individual FAD- and FMN-binding domains and determined the midpoint potentials of the flavin cofactors (*15*). The midpoint reduction potentials of the four redox couples ($FAD_{ox/sq}$, $FAD_{sq/hq}$, $FMN_{ox/sq}$, $FMN_{sq/hq}$) favors (as with the other mammalian diflavin reductases) electron transfer in the direction NADPH → FAD → FMN. Although the midpoint potentials of the four couples fall within the range of the other mammalian diflavin enzymes, this range for MSR is more compressed, and might lead to altered kinetic properties.

Prior stopped-flow and steady-state kinetic studies of individual members of the diflavin reductase family have revealed major differences in electron-transfer rates and mechanism. For example, CPR (*16*) and NOS (*17*) are able to reduce ferricyanide and cytochrome *c* at rates 25- to 100-fold greater than NR1 (*12*) and MSR (*2*). The variation in steady-state turnover numbers reported for the NADPH-dependent reduction of nonphysiological electron acceptors is potentially reflected in their respective pre-steady rate constants of flavin reduction. Reduction of the isolated FAD-domain of NR1 by NADPH occurs at 1 s^{-1} (*18*). By contrast, stopped-flow traces following absorbance changes for NOS and CPR are multiphasic with faster observed rate constants of flavin reduction (*19*−*21*). It has been suggested for CPR and rat neuronal NOS that the rate of $NADP^+$ release from reduced enzyme contributes to the overall rate of flavin reduction observed in stopped-flow absorbance studies. In addition to permitting further reduction by a second molecule of NADPH, release of $NADP^+$ from the reduced enzyme displaces the equilibrium distribution of enzyme species toward that of reduced enzyme (see ref *20* for more detailed discussion).

The fact that the turnover number for MSR catalyzed NADPH-dependent reduction of nonphysiological electron acceptors is similar to NR1 (*2*, *22*) suggests that in vivo both enzymes are kinetically compromised compared with NOS and CPR. However, reoxidation of the CPR FAD domain by ferricyanide at steady-state is *faster* than the flavin reduction rate (which is gated by the rate of $NADP^+$ release) observed in stopped-flow studies. This indicates that the electron acceptor receives electrons from the reduced enzyme−$NADP^+$ complex, thus bypassing the rate-limiting release of $NADP^+$ from this complex (*18*−*19*). Analysis of steady-state reactions with nonphysiological electron acceptors is thus potentially misleading when characterizing the overall kinetic behavior of the enzyme. With this complication in mind, we have performed a detailed study of flavin reduction using stopped-flow methods, to enable detailed comparison with similar studies performed with CPR, NOS, and NR1.

EXPERIMENTAL PROCEDURES

Materials. Methyl viologen, NADPH, and $NADP^+$ were from Sigma. Ethanol-d_6 was purchased from Aldrich. *Thermoanaerobium brokii* alcohol dehydrogenase was supplied by Fluka, and yeast alcohol dehydrogenase was from Calbiochem.

Preparation of FAD Domain, MSR, and [4(R)-^{2}H]NADPH. Human MSR (I22/S175 variant) and the individual FAD domain (residues 163−698) were cloned into the pGEX4T-1 vector. The proteins were expressed in *E. coli* BL21(DE3) and purified as previously described (*15*). The concentrations of the FAD domain and full-length MSR were determined by the absorbance value at 454 nm using the extinction coefficient of 11 300 and 21 600 M^{-1} cm^{-1}. [4(*R*)-^{2}H]-NADPH (A-side NADPD) was synthesized enzymatically and isolated using a previously described method (*20*, *23*). Fractions from the Q-Sepharose column with an A_{260}/A_{340} ratio < 2.4 containing [4(*R*)-^{2}H]NADPH were collected, lyophilized, and used for stopped-flow studies.

Stopped-Flow Kinetic Measurements. Stopped-flow studies were performed using an Applied Photophysics SX.17 MV stopped-flow spectrophotometer under anaerobic conditions. The sample-handling unit of the stopped-flow instrument was contained within a Belle Technology glovebox. Transient kinetic experiments were performed in 50 mM potassium phosphate buffer, pH 7.0, which was made anaerobic by extensive bubbling with argon. Immediately prior to the stopped-flow experiments, protein samples were fully oxidized by the addition of a small volume of excess potassium ferricyanide. The concentrated protein samples, in a total volume of 1−2 mL, were admitted to the glovebox and ferricyanide and oxygen were removed by filtering the sample over a 10 mL BioRad Econo-Pac 10 DG column (15 × 60 mm) equilibrated with anaerobic 50 mM potassium phosphate buffer, pH 7.0. For studies of hydride transfer to $NADP^+$ from two-electron reduced FAD domain or four-electron reduced MSR, proteins were reduced with a stoichiometric amount of dithionite in the presence of methyl viologen as a redox mediator. The molar ratio of the protein to methyl viologen was 10. Reduced protein was then used immediately in stopped-flow studies. Unless otherwise stated, the concentration of the protein sample in the reaction cell was 10 μM for single-wavelength and 25 μM for multiple wavelength photodiode array studies.

Stopped-flow multiple wavelength absorption studies were carried out using a photodiode array detector and X-SCAN software (Applied Photophysics Ltd.). Spectral intermediates formed during protein reduction were resolved by singular value decomposition (SVD) of the spectra acquired over 1 s (FAD domain) or 200 s (MSR) using PROKIN software (Applied Photophysics Ltd.). In single-wavelength studies, NADPH reduction of the FAD domain and full-length MSR was observed at 454 nm. Stopped-flow transients were found to be biphasic for full-length MSR over 10 s and were fitted using the standard double-exponential equation (eq 1).

$$A = C_1 e^{-k_{obs1}t} + C_2 e^{-k_{obs2}t} + b \quad (1)$$

Table 1: Rate Constants for the Reductive Half-Reaction of Human Methionine Synthase Reductase

rate constant	k_{lim} (s^{-1})	isotope effect k_{lim}^H/k_{lim}^D	K (μM)
k_{lim}^H [a]	23.0 ± 0.2		45.1 ± 1.8
k_{lim}^D [a]	9.7 ± 0.3	2.2 ± 0.1	37.4 ± 3.6
k_{lim}^H [b]	24.8 ± 0.3		57.2 ± 2.6
k_{lim}^D [b]	14.7 ± 0.3	1.7 ± 0.1	53.2 ± 3.9
k_{lim}^H [c]	21.9 ± 0.3		56.0 ± 3.4
k_{lim}^H [d]	20.9 ± 0.3		43.6 ± 2.9
k_{lim}^H [e]	2.8 ± 0.1		52.8 ± 5.2

[a] Determined from a fit of eq 3 to data shown in Figure 4B. [b] Determined from a fit of eq 3 to data shown in Figure 5B. [c] Determined from a fit of eq 3 to data shown in the inset in Figure 7A. [d] Determined from a fit of eq 3 to data shown in the inset in Figure 7B. [e] Determined from a fit of eq 3 to data shown in the inset in Figure 8A.

where k_{obs1} and k_{obs2} are the observed rate constants for the fast and slow phases, respectively, C_1 and C_2 are their relative amplitudes, and b is the final absorbance. Stopped-flow traces at 600 nm showed a rapid small increase in absorbance followed by a slower and larger decrease in absorbance, reporting on the formation and decay of an oxidized enzyme−NADPH charge-transfer species. The observed rate constants for these two phases were determined by fitting the transients using eq 2.

$$A = \frac{k_{obs1}}{k_{obs2} - k_{obs1}} C_1 e^{-k_{obs1}t} - C_2 e^{-k_{obs2}t} + b \qquad (2)$$

where k_{obs1} and k_{obs2} are observed rate constants for the formation and decay of the charge-transfer species, respectively, C_1 and C_2 are the respective amplitude changes, and b is the off-set value.

Analysis of photodiode array experiments for NADPH reduction of the FAD domain and full-length MSR indicated that the reverse rate constant for flavin reduction under the given reaction conditions is near zero. Hence, NADPH and [4(*R*)-^{2}H]NADPH concentration dependence profiles were fit to the following simplified hyperbolic equation.

$$k_{obs} = \frac{k_{lim}[S]}{K + [S]} \qquad (3)$$

where S is the coenzyme concentration, k_{lim} is the limiting rate constant of flavin reduction, and K is the substrate concentration at half the value of k_{lim}. $NADP^+$ concentration profiles for the reverse rate of hydride transfer were initially fit to the following expanded hyperbolic equation.

$$k_{obs} = \frac{k_f[S]}{K + [S]} + k_r \qquad (4)$$

with k_f and k_r equal to the limiting rate constants for flavin oxidation and reduction, respectively. Due to the lack of data at lower concentrations of $NADP^+$ (required to maintain pseudo-first-order conditions), a fit of eq 4 to the data in the inset of Figure 8A did not produce a reliable estimate of k_r. However, when k_f was fixed at 2.8 s^{-1} or when the value K was fixed between 40 and 60 μM, then the value of k_r was approximately zero. Hence, the data shown in Table 1 are from a fit of eq 3 to the data in Figure 8A (inset). Reduction of MSR and the FAD domain by NADPH were also analyzed by following change in tryptophan fluorescence; emission at 340 nm (excitation at 295 nm) was selected using a band-pass filter (Coherent Optics; 450 nm #35-3003).

RESULTS

Flavin Reduction Followed by Photodiode Array Spectroscopy. Stopped-flow analysis of NADPH reduction of MSR was investigated using a photodiode array detector to follow changes in the flavin spectra of the isolated FAD domain and the full-length enzyme. As with work on other diflavin reductases, the combined use of photodiode array and conventional single-wavelength spectroscopy to study kinetic phases as a function of reducing coenzyme concentration assisted in assignment of kinetic phases to mechanistic steps in reduction of MSR. This approach allowed separation of kinetic phases associated with formation of an enzyme−coenzyme charge-transfer intermediate, and the transfer of the first and second hydride from NADPH to MSR. Additionally, absorbance changes associated with development of the disemiquinoid state of full-length MSR, which is known to form under equilibrium titration conditions, were also isolated and investigated.

The FAD domain and full-length MSR were rapidly mixed with NADPH under single or double turnover conditions, respectively (20-fold excess NADPH), in an anaerobic environment at 25 °C. Reduction (shown by bleaching of the absorbance maxima at 454 nm) of the FAD domain occurred in <1 s (Figure 1A), whereas reduction of MSR occurred in ~200 s (Figure 2A). The spectra collected over 1 s (FAD domain) and 200 s (full-length MSR) from the initial mixing event were processed by SVD using PROKIN software to resolve a number of discrete spectral intermediates. For the FAD domain, the globally analyzed SVD spectra were best fitted to a one-step reversible kinetic model with two spectral species. The spectra of the two intermediates indicate that they are primarily the oxidized (A) and two-electron reduced (B) forms of the domain (Figure 1B). The rate constants for conversion of A → B and B → A were calculated to be 20.1 ± 0.0 s^{-1} and 0.017 ± 0.001 s^{-1}, respectively.

Globally analyzed SVD data for MSR were best fitted to a three-step reversible kinetic model (A → B → C → D) with four discrete spectral species (Figure 2B). Scheme 1 illustrates the reaction showing the rate constants of formation and decay of the spectral intermediates and what each intermediate may represent in terms of kinetically relevant species. It should be stressed that SVD analysis of the PDA spectra over a select time domain resolves the minimum *spectral* intermediates that form in the reaction, and not discrete *enzyme* intermediates. Consequently, a spectral intermediate, in particular one that forms in the middle of a reaction sequence, is an equilibrium distribution of enzyme species that are formed in a resolvable kinetic phase.

The conversion of spectral species A (oxidized enzyme) to spectral species B occurs at 24.9 ± 0.1 s^{-1}. The ~22% loss of the flavin absorbance maxima that accompanies this first kinetic phase suggests that approximately half of the enzyme becomes reduced to the two-electron level. This step is essentially irreversible under the conditions used in this experiment, as the rate constant for the reverse reaction is 0.0003 ± 0.0001 s^{-1}. We are unsure as to why there is partial

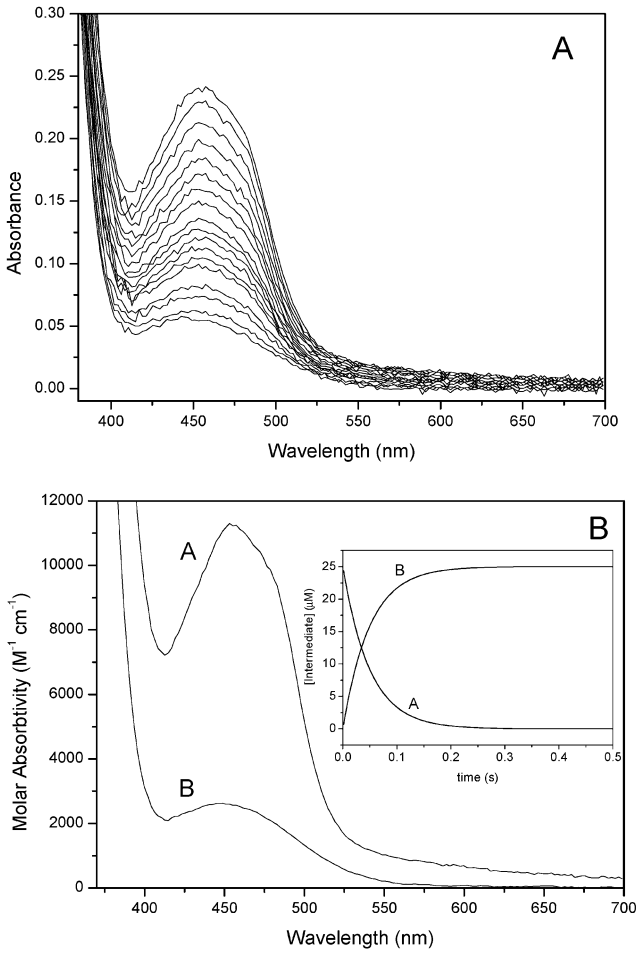

FIGURE 1: Reaction of the isolated FAD domain (25 μM) of human methionine synthase reductase with NADPH (0.5 mM) monitored by stopped-flow photodiode array spectroscopy. Conditions: 50 mM potassium phosphate buffer, pH 7.0, 25 °C. (A) Time-dependent spectral changes occurring over 1 s following rapid mixing of the FAD domain with NADPH. For clarity, only subsequent select spectra are shown. (B) Deconvoluted spectra of the intermediates resolved from time-dependent global SVD analysis of the data shown in panel A. The data shown in panel A were fitted to a reversible model of A → B with the observed rate constants of conversion of A → B and B → A occurring at 20.1 ± 0.0 s^{-1} and 1.75 × 10^{-2} ± 0.14 × 10^{-2} s^{-1}, respectively. Inset: calculated concentration profiles (over 1 s) of intermediates in the reaction of isolated FAD domain with NADPH. Profiles were obtained by fitting the data shown in panel A to a sequential A → B kinetic scheme.

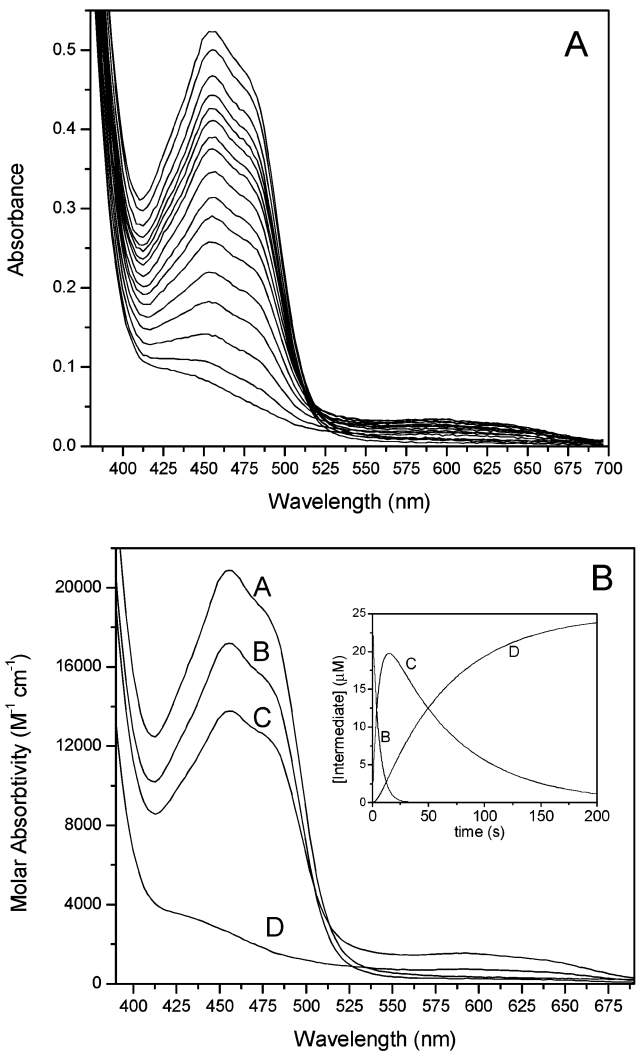

FIGURE 2: Reaction of human methionine synthase reductase (25 μM) with NADPH (0.5 mM) monitored by stopped-flow photodiode array spectroscopy. Conditions: as for Figure 2. (A) Time-dependent spectral changes occurring over 200 s following rapid mixing of MSR with NADPH. For clarity, only subsequent select spectra are shown. (B) Deconvoluted spectra of the intermediates resolved from time-dependent SVD analysis of the data shown in panel A. The data, shown in panel A, were fitted globally to a three-step reversible model of A ↔ B ↔ C ↔ D. The following are the observed rate constants (s^{-1}) obtained from the analysis: A → B, 24.9 ± 0.1; B → A, 3.2 × 10^{-4} ± 1.4 × 10^{-4}; B → C, 0.18 ± 0.00; C → B, 1.7 × 10^{-3} ± 0.1 × 10^{-3}; C → D, 1.6 × 10^{-2} ± 0.03 × 10^{-2}; D → C, 1.1 × 10^{-4} ± 0.1 × 10^{-4}. Inset: calculated concentration profiles (over 200 s) of intermediates in the reaction MSR with NADPH. Profiles were obtained by fitting the data shown in panel A to a sequential reversible model of A → B → C → D.

reduction of the enzyme at this stage given that the conversion of A → B is essentially irreversible. A possible explanation may be different modes of NADPH binding to the free full-length enzyme, one that promotes rapid hydride transfer and another that requires slower conformational movement to facilitate hydride transfer (see Discussion). The observed forward and reverse rate constants for the interconversion of spectral species B and C are 0.18 ± 0.00 s^{-1} (B → C) and 0.002 ± 0.000 s^{-1} (C → B). The formation of C involves a further decrease in absorbance at 454 nm and a small increase in absorbance at 600 nm. Judging by the absorbance at 454 nm, the majority of the enzyme is reduced at the two-electron level at the completion of this kinetic phase. A small signature at 600 nm indicates that a population of the enzyme is in the disemiquinoid (FAD_{sq}/FMN_{sq}) state, in equilibrium with FAD_{hq}/FMN_{ox} and/or FAD_{ox}/FMN_{hq} forms of MSR. At this point in the reaction scheme, it is not clear if the oxidized nucleotide is bound to the enzyme. In studies with related diflavin enzymes, it has been suggested that release of $NADP^+$ bound to enzyme containing the FAD hydroquinone is required to enable interflavin electron transfer (*20*, *24*). By analogy, this suggests for MSR that $NADP^+$ dissociates during the conversion of B to C, allowing limited interflavin electron transfer. However, we cannot demonstrate the extent by which the coenzyme influences the equilibrium between the different redox states of MSR; thus, $NADP^+$ release in principle could occur from species B or C. As such, $NADP^+$ is enclosed in parentheses in Scheme 1, and species C could comprise upward of six

Scheme 1

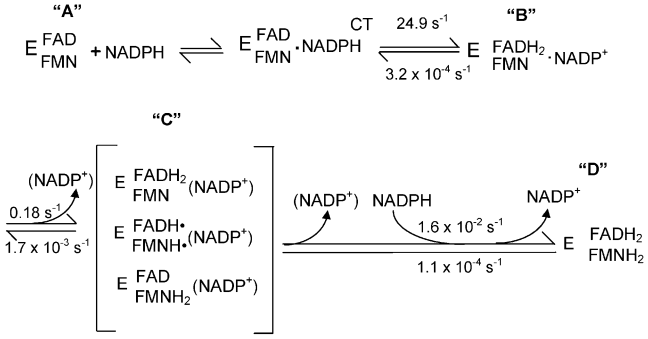

kinetically relevant species, i.e., the three different forms of two-electron reduced MSR (FAD_{hq}/FMN; FAD_{sq}/FMN_{sq}; FAD/FMN_{hq}), with and without bound $NADP^+$. The formation of MSR reduced at the level of four electrons occurs during the accumulation of spectral species D, and is represented by further bleaching of absorbance at 454 and 600 nm. The formation of spectral species D occurs with rate constants of $0.016 \pm 0.00\ s^{-1}$ (C → D) and $0.0001 \pm 0.0000\ s^{-1}$ (D → C). During this kinetic phase, the enzyme becomes fully reduced as a result of binding and oxidizing a second molecule of NADPH. Again, there is uncertainty as to whether species D is bound to $NADP^+$ (or NADPH) at the completion of this kinetic phase.

Spectral intermediates that form in the two-electron reduction of MSR were also investigated by photodiode array spectroscopy with rapid mixing of equimolar full-length enzyme and NADPH (Figure 3A). The spectra collected over 200 s were globally analyzed by SVD. The data were best fitted to a model where spectral species A (oxidized MSR) and species B (NADPH) react to form the spectral intermediate C (Figure 3B; Scheme 2). Species C is characterized by a ~22% decrease in absorbance at 454 nm compared to species A, suggesting only a subset of the enzyme molecules are reduced to the two-electron level in this first kinetic phase. In the second kinetic phase, there is additional loss of absorbance at 450 nm and a small increase in absorbance at 600 nm. The spectral intermediate at this stage (species D) is like the corresponding species C shown in Scheme 1, and thus represents an equilibrium distribution of two-electron reduced forms of MSR in different redox states (with or without bound $NADP^+$). Over an extended time scale, spectral species D irreversibly decomposes to the final spectral species E. Species E has near equal absorbance maxima at 450 and 600 nm and reflects the enzyme predominantly relaxing to the disemiquinoid state. Release of $NADP^+$ could accompany conversion of species C → D and/or D → E. SVD analysis clearly indicates that conversion of D → E is irreversible; attempts to fit the data to a reversible process generated a final spectrum that did not resemble a reduced or partially reduced flavin. The last real time spectrum taken of MSR (Figure 3A) does not overlay precisely with spectrum E (Figure 3B), in that it appears at this stage (200 s after mixing) that the enzyme has not fully relaxed to the disemiquinoid state, as the model predicts. The model is invariably more complex at this stage of the reaction sequence. Although conversion of intermediate D → E is ascribed to one irreversible step in the model, transitions to the most thermodynamically relaxed state likely encompass a sequence of disproportionation reactions not

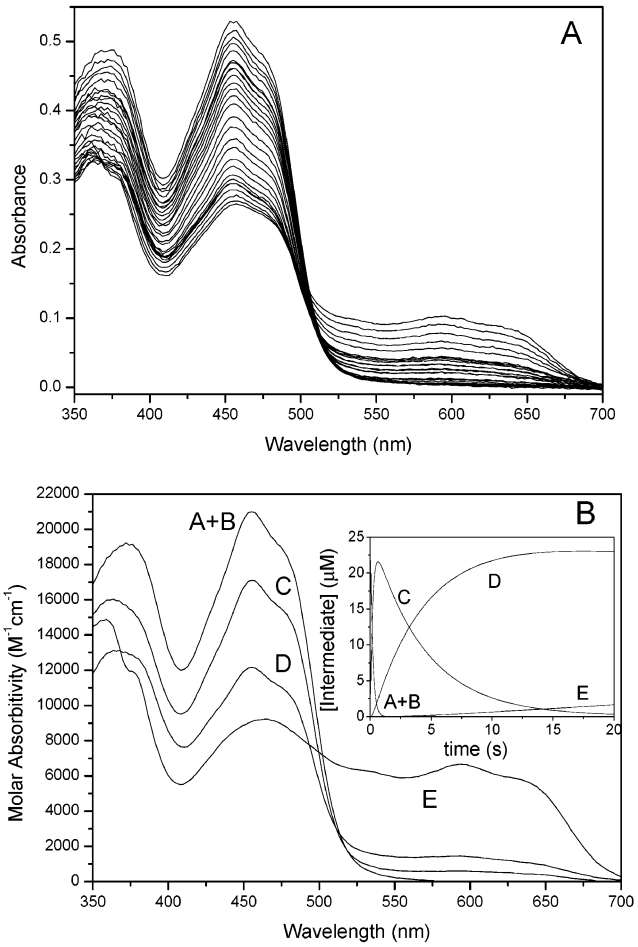

FIGURE 3: Reaction of human methionine synthase reductase (25 μM) with NADPH (25 μM) under equimolar conditions monitored by stopped-flow photodiode array spectroscopy. Conditions as for Figure 2. (A) Time-dependent spectral changes occurring over 200 s following rapid mixing of MSR with NADPH. For clarity, only subsequent select spectra are shown. (B) Deconvoluted spectra of the intermediates resolved from time-dependent SVD analysis of the data shown in panel A. The data shown in panel A were fitted globally to the following three-step model of A + B ↔ C ↔ D ↔ E. The following are the observed rate constants (s^{-1}) obtained from the analysis: A + B → C, 5.08 ± 0.01; C → A + B, $7.1 \times 10^{-3} \pm 0.9 \times 10^{-3}$; C → D, 0.23 ± 0.00; D → C, $1.7 \times 10^{-4} \pm 0.2 \times 10^{-4}$; D → E, $4.4 \times 10^{-3} \pm 0.0 \times 10^{-3}$; Inset: calculated concentration profiles (over 200 s) of intermediates in the reaction MSR with NADPH. Profiles were obtained by fitting the data shown in panel A to a sequential reversible model of A + B → C → D → E.

Scheme 2

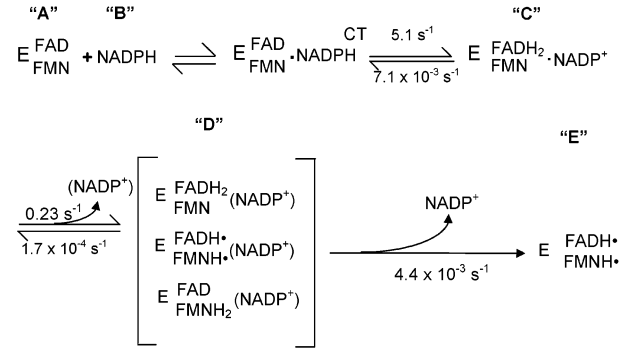

factored into the model. Alternatively, a limited amount of photobleaching of the flavin chromophores may also account for the reduced absorbance signal for the real time spectrum

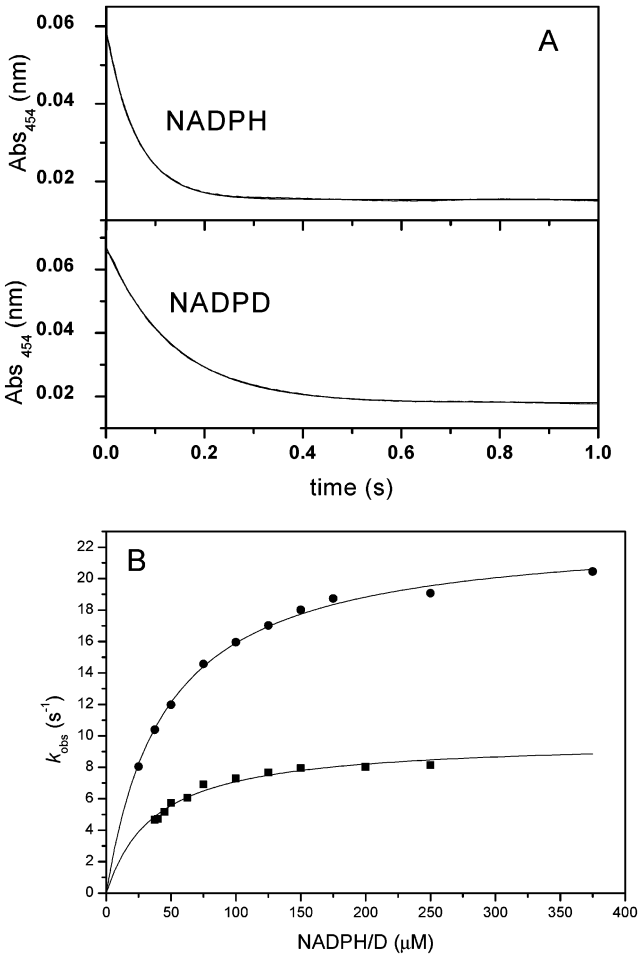

FIGURE 4: Stopped-flow single-wavelength absorbance (454 nm) transient after mixing the MSR FAD domain (5 μM) with NADPH and [4(*R*)-^{2}H]NADPH under pseudo-first-order conditions. Conditions as for Figure 2. (A) Monophasic transient obtained at 454 nm with 100 μM NADPH and with 100 μM [4(*R*)-^{2}H] NADPH. Fitting the data in panel A to a standard single-order exponential equation over 2 s yields a value of k_{obs} of 19 and 8 s^{-1} for NADPH and [4(*R*)-^{2}H]NADPH, respectively. (B) Dependence of k_{obs} on [NADPH] (●) and [4(*R*)-^{2}H]NADPH] (■) concentration. The data in panel B were fitted to eq 3 and the results are shown in Table 1.

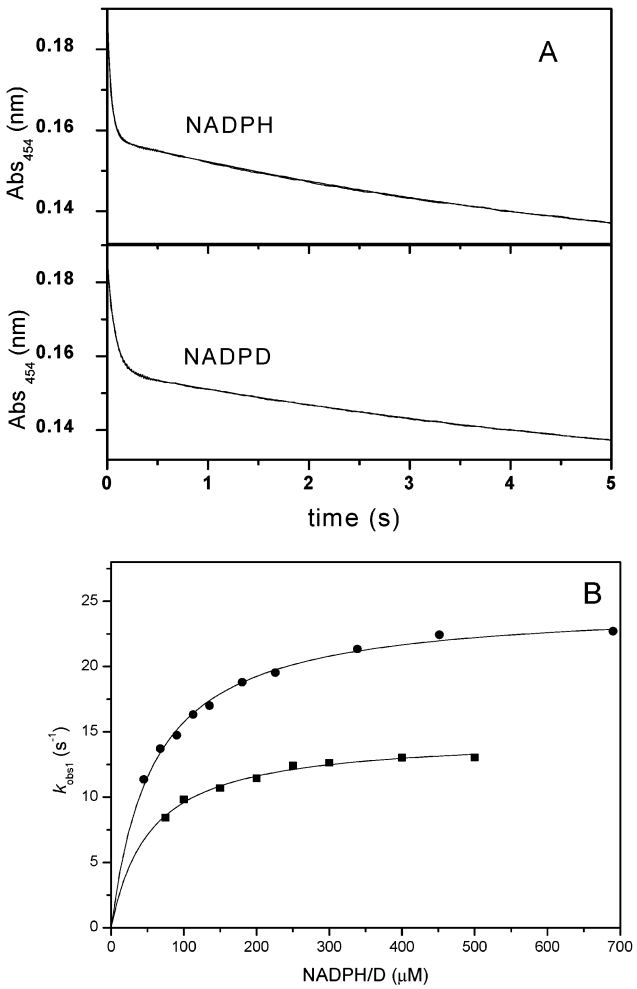

FIGURE 5: Stopped-flow single-wavelength absorbance (454 nm) trace following the mixing of MSR (10 μM) with NADPH and [4(*R*)-^{2}H]NADPH under pseudo-first-order conditions. Conditions as for Figure 2. (A) biphasic transient obtained at 454 nm with 200 μM NADPH and with 200 μM [4(*R*)-^{2}H] NADPH. Fitting the data in panel A to eq 1 over 10 s gave values of k_{obs1} and k_{obs2} for NADPH, (24.9, 0.17 s^{-1}) and [4(*R*)-^{2}H]NADPH, (13.0, 0.14 s^{-1}), respectively. (B) Dependence of k_{obs} on [NADPH] (●) and [[4(*R*)-^{2}H]NADPH] (■) concentration. The data in panel B were fitted to eq 3 and the results are shown in Table 1.

over the extended time domain of the experiment. The rate constants obtained from global fitting of spectral changes are given in the legend for Figure 3.

Single-Wavelength Stopped-Flow Studies. Single-wavelength stopped-flow absorption and fluorescence studies were performed to measure rate constants during the NADPH reduction of MSR under pseudo-first-order conditions. The measured values in the single-wavelength studies were compared to the calculated rate constants for the interconversion of spectral intermediates obtained in photodiode array experiments to access model validity. Single-wavelength absorbance transients measured at 454 nm (flavin reduction) after rapid mixing of the FAD domain with NADPH under pseudo-first-order conditions were monophasic (Figure 4A). The observed rate constant exhibited a hyperbolic saturation dependence on NADPH concentration (Figure 4B) in the pseudo-first-order regime. A fit of the data to eq 3 yielded a K of 45.1 ± 1.8 μM and a k_{lim} (maximal rate constant of flavin reduction) of 23.0 ± 0.2 s^{-1} (Table 1). The limiting rate constant is similar to the rate constant of interconversion of spectral species A to species B observed in photodiode array studies (see above). The FAD domain mixed with [4(*R*)-^{2}H]NADPH (A-side) under pseudo-first-order conditions also produced a monophasic stopped-flow trace at 454 nm. (Figure 4A). Stopped-flow traces were fit to a single-exponential function and observed rate constants showed a hyperbolic dependence on [4(*R*)-^{2}H]NADPH concentration with a K of 37.4 ± 3.6 μM and a k_{lim} of 9.7 ± 0.3 s^{-1} (Figure 4B). The primary kinetic isotope effect on k_{lim} ($^D k_{lim}$) was calculated to be 2.2 ± 0.1 indicating that hydride transfer is a part of this observed kinetic phase.

Figure 5A shows stopped-flow absorbance traces at 454 nm following rapid mixing of full-length MSR with 20-fold excess of NADPH. The traces report the rate constants associated with flavin reduction and were biphasic over a 10 s time domain (k_{obs1} = 24.9 s^{-1} and k_{obs2} = 0.17 s^{-1}). These two observed rate constants over the same time scale match the observed rate constants for transition of spectral intermediate A → B and B → C in the photodiode array experiment shown in Figure 2. Consistent with Scheme 1,

reduction to the final equilibrium position occurred over 200 s, but the multiphasic transients proved difficult to fit to a higher order exponential equation. Stopped-flow traces were also biphasic over 10 s following rapid mixing of MSR with [4(*R*)-^{2}H]NADPH under pseudo-first-order conditions (Figure 5A). A fit of the traces to eq 1 gave values of k_{obs1} (13.0 s^{-1}) and k_{obs2} (0.14 s^{-1}). As with the FAD domain, the rate of flavin reduction in MSR was monitored as a function of NADPH or [4(*R*)-^{2}H]NADPH concentration in the pseudo-first-order regime. Figure 5B shows that the value of k_{obs1} increases hyperbolically with coenzyme concentration. A nonlinear least-squares fit of eq 3 to the data gave *K* and k_{lim} values for NADPH (57.2 ± 2.6 μM; 24.8 ± 0.3 s^{-1}) and [4(*R*)-^{2}H]NADPH (53.2 ± 3.9 μM; 14.7 ± 0.3 s^{-1}). Hydride transfer occurs in the fast kinetic phase as the primary KIE on k_{lim} ($^D k_{lim}$) was calculated to be 1.7 ± 0.1. Limiting rate constants for full-length MSR and the isolated FAD domain are collected in Table 1.

Single-wavelength stopped-flow studies at 600 nm were also performed on the FAD domain and full-length MSR to investigate in more detail the absorbance changes that were observed at this wavelength with photodiode array spectroscopy. Figure 6A shows the stopped-flow trace resulting from rapid-mixing of 20-fold excess of NADPH with the FAD domain. The trace clearly shows a rapid "up" phase followed by a slower "down" phase with twice the amplitude change. As the two kinetic phases have discrete amplitude changes, the traces were fitted to eq 2 to extract observed rate constants for the two portions of the transient. A fit of eq 2 gave k_{1obs} of 120 s^{-1} and k_{2obs} of 19 s^{-1}, which likely represent the formation and decay of a charge-transfer species. Since the amplitude of the "up" phase approximates only half of the amplitude of the "down" phase, this leaves the possibility that the earlier part of the transient is preceded by a more rapid phase that occurs within the dead time (1 ms) of the stopped-flow instrument. However, when the reaction was performed at lower temperature (7 °C) k_{1obs} decreased to 46 s^{-1} and k_{2obs} to 4 s^{-1} without a change in relative amplitudes suggesting the absence of an earlier phase at 600 nm (data not shown).

Full-length MSR rapidly mixed with 20-fold excess of NADPH gave similar stopped-flow traces at 600 nm as the FAD domain under the same conditions (Figure 6B). A rapid "up" phase with the diminished amplitude is followed by a slower "down" phase showing the formation and decay of charge-transfer character. The absorbance signal then climbs again over a longer time domain reflecting the formation of the disemiquinoid state. A fit of eq 2 to the trace over 0.5 s gave values for k_{1obs} (100 s^{-1}) and k_{2obs} (20 s^{-1}). Charge-transfer signature was not observed in the long wavelength region using photodiode array detection for full-length MSR (Figure 2) or the isolated FAD domain (Figure 1) because the absorbance signal is relatively small, and photodiode array detection has an inherently large signal-to-noise ratio. Furthermore, the kinetic phase is relatively rapid and the first diode array scan occurs at 1.28 ms, leading to the loss of a small amount (~13%) of the charge-transfer signal prior to spectrum acquisition.

Stopped-flow fluorescence analysis was also used to monitor hydride transfer in MSR and the FAD domain. The crystal structure of rat CPR indicates a tryptophan residue resides over the *re*-face of the isoalloxazine ring of FAD

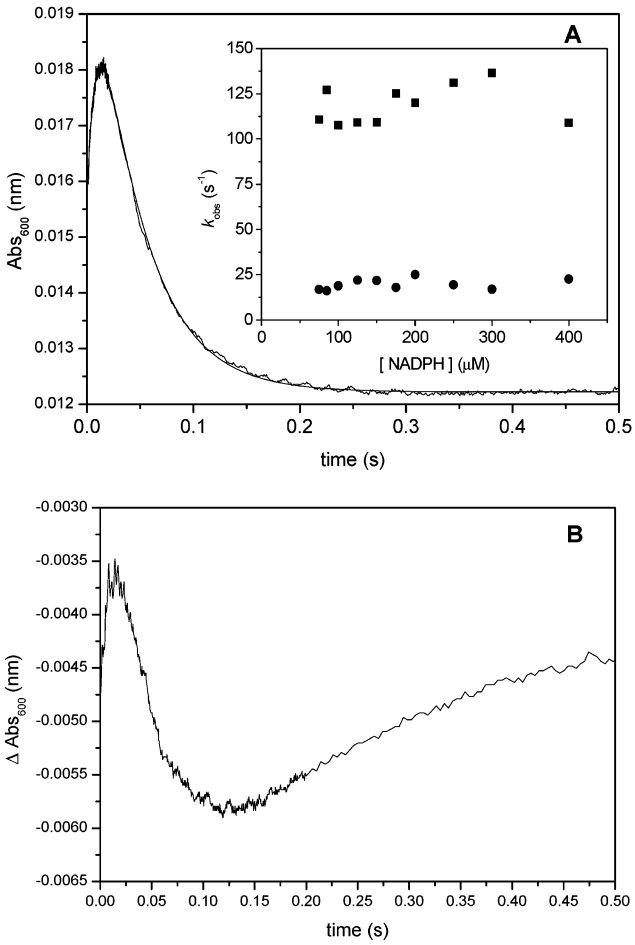

FIGURE 6: Transient obtained at 600 nm following rapid mixing of NADPH and the FAD domain (10 μM; panel A) or MSR (10 μM; panel B) under pseudo-first-order conditions. Conditions as for Figure 2. The trace was fit to eq 2 which describes a transient with a monophasic "up" phase followed a monophasic "down" phase with discrete amplitudes. (A) The observed rate constants for the fast "up" (k_{obs1}) and "down" (k_{obs2}) phases are ~120 and 19 s^{-1}. Inset: NADPH concentration dependence on k_{obs1} and k_{obs2}. (B) The observed rate constants for the fast "up" (k_{obs1}) and "down" (k_{obs2}) phases are 100 and 20 s^{-1}.

(*25*). This aromatic residue must flip away from the ring to allow hydride transfer from the nicotinamide coenzyme. The movement of the tryptophan is accompanied by a change in the fluorescence signal of the residue and this feature of the mechanism has also been used to monitor hydride transfer in human CPR (*19*). Sequence alignment with CPR suggests that Trp697 is the corresponding residue in MSR. Figure 7A shows the stopped-flow trace (excitation at 295 nm) following mixing of the FAD domain with 20-fold excess NADPH. The monophasic transient was fit to a single-exponential function and the calculated k_{obs} was 18.0 s^{-1}, in agreement with the observed rate constant of flavin reduction observed at 454 nm (Figure 4A) and the photodiode array experiment (Figure 1). The inset of Figure 7A shows that the value of k_{obs} increases in a hyperbolic fashion with NADPH concentration in the pseudo-first-order regime. A fit of eq 3 to the concentration profile yields values for *K* of 56.0 ± 3.4 μM and k_{lim} = 21.9 ± 0.3 (Table 1) that agree with the values determined from single-wavelength stopped-flow studies at 454 nm (Figure 4B). Full-length MSR mixed with NADPH under the same conditions as the FAD domain yielded a similar monophasic trace with k_{obs} = 19 s^{-1} (Figure

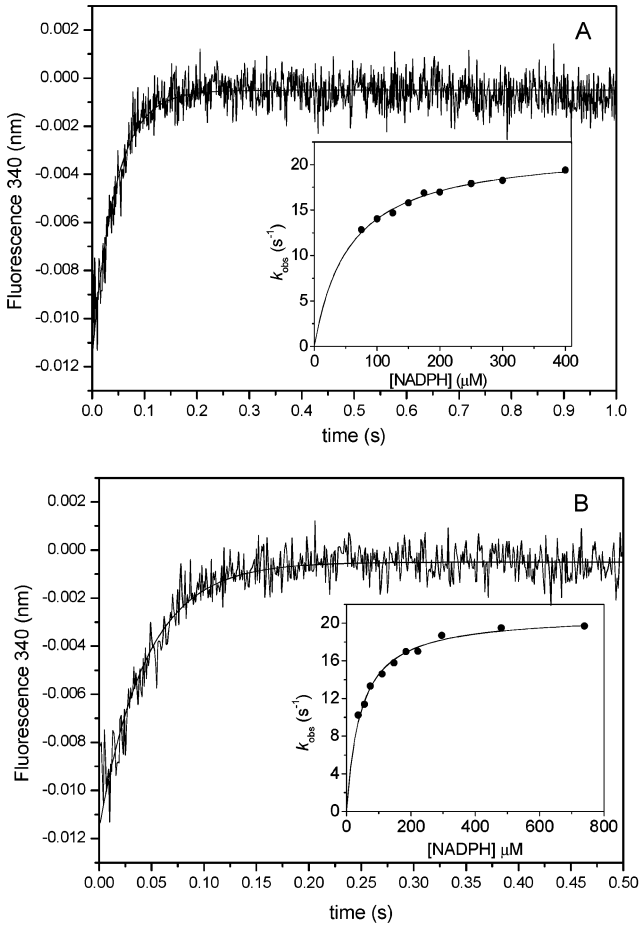

FIGURE 7: Tryptophan fluorescence traces following for the reduction of the FAD domain by NADPH. Conditions as for Figure 2. The increase in tryptophan fluorescence (excitation at 295 nm) after rapid mixing of the FAD domain (10 μM; panel A) or MSR (10 μM, panel B) with NADPH (200 μM) was monophasic and was fitted to a single-exponential function (k_{obs} = 18 s^{-1} for panel A and k_{obs} = 19 s^{-1} for panel B). Insets: The NADPH concentration dependence on k_{obs1}. The data were fitted to eq 3 and are shown in Table 1.

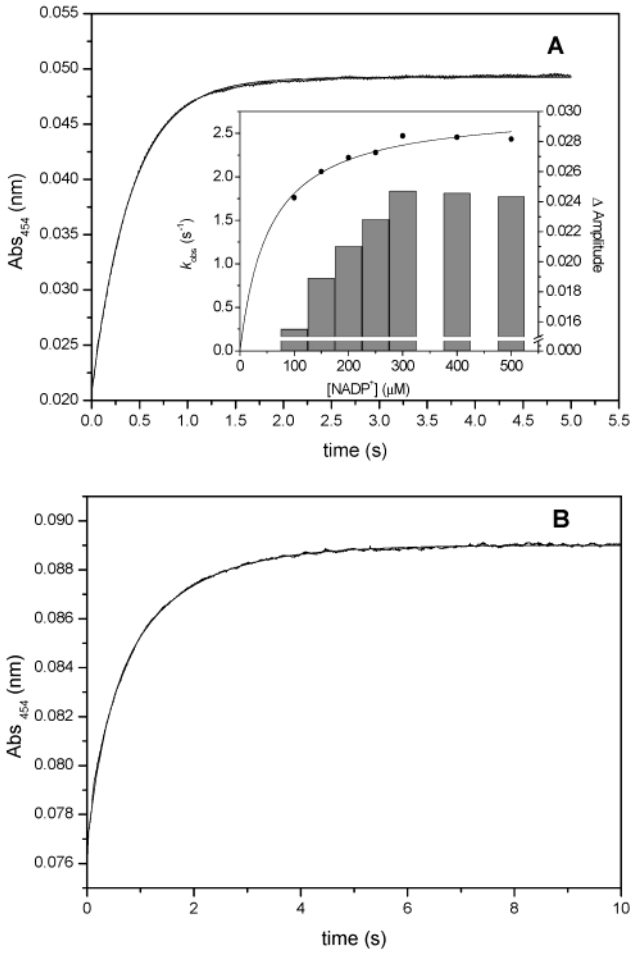

FIGURE 8: Single-wavelength absorbance (454 nm) trace for the reaction of dithionite-reduced FAD domain and MSR with $NADP^+$. Conditions as for Figure 2. (A) Absorbance trace after rapid mixing of $NADP^+$ (200 μM) with dithionite-reduced FAD domain (10 μM). The trace was monophasic and was fitted to a single-exponential function (k_{obs} of 2.4 s^{-1}). Inset: $NADP^+$ concentration dependence on k_{obs} (●) and the corresponding amplitude (histogram). The data were fit to eq 3, and the results are shown in Table 1. (B) Absorbance trace after rapid mixing of $NADP^+$ (200 μM) with dithionite-reduced MSR (10 μM). The traces were biphasic and was fitted to a double exponential function [k_{obs1} = 1.4 s^{-1}; k_{obs2} = 0.4 s^{-1}].

7B), which is similar to the fast observed rate constant (k_{obs1}) determined from stopped-flow traces at 454 nm under the same conditions. A fit of the k_{obs}−NADPH concentration data to eq 3 gave values for K (43.6 ± 2.9 μM) and k_{lim} (20.9 ± 0.3 s^{-1}).

Reverse of Hydride Transfer. The reversibility of hydride transfer has been demonstrated in CPR (*19*) and NR1 (*18*). For these enzymes, where the $FAD_{ox/hq}$ redox couple is more electronegative [−340 mV for NR1; *8*; −371 mV for CPR; *26*] in relation to NADPH (−320 mV), hydride transfer was shown to be faster in the reverse direction (FAD_{hq} to $NADP^+$). If the redox potentials of the coenzyme and flavin influence rates of hydride transfer, then reverse hydride transfer in MSR is expected to be slower than in the forward direction. The FAD domain reduced at the level of two electrons with dithionite under anaerobic conditions was rapidly mixed with 20-fold excess $NADP^+$ and the rate of flavin oxidation was followed at 454 nm. Figure 8A shows a monophasic increase in absorbance at this wavelength, and a fit of the data to a single-exponential function generates an observed rate constant of 2.4 s^{-1}. Figure 8A inset shows that k_{obs} has a hyperbolic dependence on $NADP^+$ concentration and reveals that the total change in amplitude also increases with oxidized coenzyme concentration. A fit of eq 3 to the k_{obs} data yields a K of 52.8 ± 5.2 μM and a k_{lim} of 2.8 ± 0.1 s^{-1} (Table 1). Figure 8B shows the 454 nm absorbance trace after rapid mixing of $NADP^+$ (200 μM) with MSR (10 μM) reduced at the four-electron level with dithionite. The trace was biphasic and a fit to a double exponential function gave values for k_{obs1} (1.4 s^{-1}) and k_{obs2} (0.4 s^{-1}). Data for the FAD domain and full-length MSR are summarized in Table 1.

The observed rate constant (2.4 s^{-1}) for reverse hydride transfer from the reduced FAD domain to $NADP^+$ (200 μM) is ∼100-fold greater than the calculated rate constant for conversion of spectral species B to species A (0.017 s^{-1}) calculated from the photodiode array experiment shown in Figure 1. As the conversion of B → A also reflects reverse hydride from the reduced FAD domain to $NADP^+$, the discrepancy between these rate constants is of interest. In the single-wavelength study, the reduced protein was mixed with a 20-fold excess of $NADP^+$, whereas in the photodiode array experiment the oxidized FAD domain was mixed with

20-fold excess of NADPH, and thus the reaction conditions are not the same. Indeed, when the FAD domain reduced at the two-electron level with dithionite was mixed with a mixture of NADPH and $NADP^+$ (19:1 ratio, in which $NADP^+$ was equimolar with the protein) a measurable change in absorbance was not detected under these reaction conditions. This is consistent with excess NADPH favoring enzyme reduction in the photodiode array experiment shown in Figure 1. Clearly, the presence of excess reducing or oxidizing nucleotide can affect the kinetic behavior of MSR and it is expected that NADPH and $NADP^+$ will compete for a common binding site in the same redox state of MSR. Thus, the different ratios and concentrations of NADPH and $NADP^+$ in the photodiode array and single wavelength studies likely contribute to different rates of hydride transfer from $FADH_2$ to $NADP^+$.

DISCUSSION

The mechanism and thermodynamics of electron transfer in the mammalian diflavin enzymes, NOS, CPR, and recently NR1, have been the subject of intensive investigation by a number of research groups (*18*−*21*, *26*, *27*). Here we have provided an analysis of the kinetic behavior of electron flow in the fourth known member of the human diflavin reductase family, MSR. Coupled with the values of the midpoint potentials of the flavin cofactors, now reported for all four members (*15*, *18*, *26*, *27*), we are able to relate the varying kinetic behavior in terms of thermodynamic differences within the family of diflavin enzymes.

Initially, photodiode array spectroscopy was used to monitor the time-resolved flavin spectra of the FAD domain following rapid mixing with a 20-fold excess of NADPH. Reduction of the protein occurred within 1 s, and time-resolved spectra were best fitted to a single-step and reversible kinetic model, in which the two predominant species are the oxidized and the two-electron reduced forms of the FAD domain (Figure 1B). The flavin reduction rate constant (20 s^{-1}) is equivalent to that observed in single-wavelength (454 nm) stopped-flow absorbance and fluorescence experiments. The calculated rate constants determined from photodiode array experiments are consistent with those obtained in single-wavelength studies. With full-length MSR, conventional single-wavelength stopped-flow studies at 454 nm (following flavin reduction) are also consistent with data collected using photodiode array detection. In contrast, formation of the charge-transfer complex for the FAD domain and full-length MSR was not observed at 600 nm by photodiode array detection because the kinetic phase is relatively fast and the signal amplitude is very small. The longer acquisition time in photodiode array mode coupled with the inherent noise associated with this detection method likely accounts for the lack of observable signal associated with the charge-transfer species.

When the CPR FAD domain is mixed with 20-fold excess NADPH, the final flavin spectrum observed using photodiode array detection indicates that the protein is not reduced to the same extent as the MSR FAD domain (*24*). The midpoint potential of the $FAD_{ox/hq}$ couple for MSR (−269 mV; *15*) is ∼60 mV more electropositive than CPR (−329 mV; *26*) and ∼50 mV more electropositive than NADPH. The thermodynamics of the MSR system therefore favor the formation of the reduced flavin−$NADP^+$ complex to a greater extent than in CPR, providing a rationale for the greater extent of FAD reduction in the MSR FAD domain.

In contrast to the isolated FAD domain of MSR, multiple wavelength stopped-flow analysis of MSR reduction by NADPH reveals four discrete spectral intermediates accumulate in the reductive half-reaction. The additional intermediates reflect in part electron transfer to the FMN cofactor and a second hydride transfer event. Under pseudo-first-order conditions, the rate constant (25 s^{-1}) approximates that observed for the FAD domain under the same conditions. However, the amplitude change associated with the formation of species B in the reduction of MSR by NADPH indicates that only ∼50% of the enzyme sample is reduced at the two-electron level, which is surprising given the essentially irreversible nature of the reaction under the conditions used in the stopped-flow studies. A possible explanation is that the NADPH-binding site might be more conformationally dynamic in the full-length enzyme and can thus accommodate different binding modes for the coenzyme. One binding mode might facilitate more rapid formation of a charge-transfer complex and subsequent hydride transfer while binding in another mode might involve slower conformational changes to facilitate hydride transfer. This aspect of the kinetic behavior of MSR warrants further investigation.

Photodiode array experiments with MSR indicate that the calculated rate constant of the first kinetic phase for flavin reduction decreases 5-fold (5 s^{-1}) when the NADPH concentration is reduced to equimolar with enzyme compared with reactions performed in the pseudo-first-order regime. This reflects attenuation of the bimolecular association of enzyme and NADPH as a result of lower coenzyme concentration. The observed rate constant (0.2 s^{-1}) for the conversion to the third spectral species is the same irrespective of NADPH concentration, reflecting a unimolecular process within the enzyme−substrate complex. The limited formation of the disemiquinoid species in the conversion of species B → C (Scheme 1) or C → D (Scheme 2) indicates some redistribution of electrons between the flavins. The conversion of the two-electron reduced form of MSR (species C) to the four-electron reduced state (species D) occurs slowly at 0.016 s^{-1} (Scheme 1). This might be attributable to the slow release of $NADP^+$ required for the binding of a second NADPH coenzyme. Alternatively, the slow rate of reduction to the four-electron level might reflect the equilibrium distribution prior to this kinetic phase since two electrons would need to redistribute to the FMN (forming FMN hydroquinone) to enable the second hydride transfer from NADPH. The values of the four redox couples for MSR (*15*) are more compressed compared to CPR (*26*) and NOS (*27*), and this might lead to relatively slow interflavin electron transfer to form the FMN hydroquinone in two-electron reduced MSR. Additionally, as in human CPR, interflavin electron transfer is likely to be conformationally gated. Temperature jump relaxation spectroscopy studies of human CPR have demonstrated that the rates of internal electron transfer are sensitive to solution viscosity (*28*). It is possible that the extended interdomain linker in MSR imposes a greater degree of relative flexibility for the flavin-binding domains, which in turn might impact on the rates of interflavin electron transfer. Clearly, the potential mechanistic

reasons for the very slow reduction of MSR to the four-electron level are numerous and will require further and detailed experimental investigation. In stopped-flow studies of MSR reduction by equimolar NADPH, formation of the final spectral species (species E, Scheme 2) represents enzyme equilibrating predominantly to the disemiquinoid state. This is expected from the known redox potentials of the flavin couples in MSR (*15*) and is consistent with similar observations made with CPR (*19*) and NOS (*20*).

Single-wavelength absorbance changes at 600 nm showed that the formation of a charge-transfer complex between NADPH and the FAD domain occurs at ~120 s^{-1}. This rate constant appears to be independent of NADPH concentration over the range used in the stopped-flow experiments, but the small signal and thus by necessity the approximate fitting of data in the "up" phase complicates detailed analysis in the early time domain. As the calculated rate constant of flavin reduction is dependent on NADPH concentration the rate constant for the decay of the charge-transfer signature should also show some dependence on NADPH concentration. The large errors in fitting to the complex transients obtained at 600 nm, coupled with the expected small changes in the rate constant upward from 75 μM NADPH (see Figures 4B and 5B for NADPH concentration effects on the observed rate constants of flavin reduction at 454 nm) might account for the lack of detectable dependence of the rate constant on coenzyme concentration, although this might warrant further investigation in future work. Stopped-flow absorbance traces at 600 nm for full-length MSR also show the formation and decay of a charge-transfer band at approximately the same rates as the FAD domain. The rate constant for the decay of the charge-transfer complex (19 s^{-1}) is similar to the observed rate constant of hydride transfer (24 s^{-1}). Similar stopped-flow studies with NOS and CPR also indicate rapid formation of charge-transfer species, the decay of which is linked to flavin reduction (*19*, *20*).

For each member of the diflavin reductase family, the FAD/NADPH binding domain is structurally and functionally similar to that found in FNR. However, the physiological direction of hydride transfer in FNR is from the reduced flavin to $NADP^+$. As for other members of the diflavin reductase family, we have shown that the isolated FAD domain and full-length MSR can transfer a hydride equivalent from reduced enzyme to $NADP^+$. With two-electron-reduced FAD domain, hydride transfer occurs in a single kinetic phase with a limiting rate constant of 2.8 s^{-1}. The corresponding stopped-flow transients for full-length MSR are biphasic (1.4 and 0.4 s^{-1}). The calculate rate constant of the first phase in MSR is similar to that measured for the isolated FAD domain, and we attribute this phase to the first hydride transfer from $FADH_2$ to $NADP^+$. The second phase reports on the second hydride transfer following electron redistribution from FMN to FAD to form the FAD hydroquinone.

The observed rate constant for hydride transfer, both in the forward and reverse direction, elicited a hyperbolic dependence on NADP(H/D) concentration consistent with a multistep mechanism involving rapid binding/conformational step(s) that precede slower kinetic step(s). MSR is the first of the four human diflavin reductases to elicit this type of hyperbolic dependence on NADPH concentration. With NOS, the kinetic phase describing the establishment of the initial equilibrium between the enzyme charge-transfer species and the two-electron reduced enzyme-bound to $NADP^+$ did not show any dependence on NADPH concentration (*20*). However, the relatively large errors associated with measurement of the observed rate constant prevented rigorous assessment of the concentration dependence. Similarly, the observed rate constant of hydride transfer in the isolated FAD domain of human NR1 has been shown to be independent of NADPH concentration using stopped-flow studies (*18*). CPR elicits the most anomalous behavior; following establishment of an initial equilibrium between two-electron reduced enzyme bound to $NADP^+$ and an oxidized enzyme-NADPH charge-transfer species, the flavin reduction rate is independent of NADPH concentration in the pseudo-first-order regime, but as NADPH concentration becomes equimolar with enzyme, the observed rate constant increases (*19*). Taken together with evidence from double mixing stopped-flow studies of the W676H mutant of CPR, this has been interpreted as CPR having a second noncatalytic binding site for NADPH, occupation of which attenuates the rate of flavin reduction by hindering the release of $NADP^+$ (*19*).

We have shown that the individual FAD domain and full-length MSR enzymes have similar limiting rates of hydride transfer, comparable midpoint potentials for the $FAD_{ox/sq}$ and the $FAD_{sq/hq}$ couples (*15*), and similar values for *K* (Table 1). Thus, the FAD domain is able to retain similar kinetic and thermodynamic properties when separated from the FMN domain. The only notable difference between the isolated FAD domain and the full-length enzyme is observed in the relative amplitude changes associated with the first kinetic phase for flavin reduction. As mentioned above, the more complex conformational dynamics of full-length MSR might invoke different binding states for NADPH that result in two separate kinetic phases describing MSR reduction to the two-electron level. Nevertheless, the overall similar behavior of the isolated FAD domain and full-length MSR reveals the value of studying isolated domains to gain additional mechanistic insight into the properties of more complex redox enzymes.

In summary, aspects of the reductive half-reaction of MSR are shared with other members of the diflavin reductase family. These include rapid formation of NADPH−enzyme charge-transfer complex, fluorescence changes suggesting movement of a tryptophan residue to allow hydride transfer from NADPH to FAD, and the ability to catalyze reverse hydride transfer to $NADP^+$. However, there are also notable differences between family members, including the hyperbolic dependence of the flavin reduction rate on NADPH concentration in MSR, relative stabilization of the disemiquinoid form of the enzymes during stopped-flow studies and the multiphasic nature of stopped-flow kinetic traces. The work described in this paper forms a basis for more detailed studies aimed at identifying different conformational states in MSR and investigating their role in electron transfer. Structural comparison of MSR with CPR, NOS, and NR1 should provide important clues as to how these variations in kinetic and mechanistic behavior relate to structural differences in the enzymes, and this work along these lines is currently in hand.

REFERENCES

1. Leclerc, D., Wilson, A., Dumas, R., Gafuik, C., Song, D., Watkins, D., Heng, H. H., Rommens, J. M., Scherer, S. W., Rosenblatt, D. S., and Gravel, R. A. (1998) *Proc. Natl. Acad. Sci. U.S.A. 95*, 3059−3064.
2. Olteanu, H., and Banerjee, R. V. (2001) *J. Biol. Chem. 276*, 35558−35563.
3. Banerjee, R. V., Frasca, V., Ballou, D. P., and Matthews, R. G. (1990) *Biochemistry 29*, 11101−11109.
4. Banerjee, R. V., Harder, S. R., Ragsdale, S. W., and Matthews, R. G. (1990) *Biochemistry 29*, 1129−1135.
5. Wilson, A., Leclerc, D., Rosenblatt, D. S., and Gravel, R. A. (1999) *Hum. Mol. Genet. 8*, 2009−2016.
6. Refsum, H., Ueland, P. M., Nygard, O., and Vollset, S. E. (1998) *Annu. Rev. Med. 49*, 31−62.
7. Masser, P. A., Taylor, L. M., Jr., and Porter, J. M. (1994) *Ann. Thorac. Surg. 58*, 1240−1246.
8. Steegers-Theunissen, R. P., Boers, G. H., Trijbels, F. J., Finkelstein, J. D., Blom, H. J., Thomas, C. M., Borm, G. F., Wouters, M. G., and Eskes, T. K. (1994) *Metabolism 43*, 1475−1480.
9. Mills, J. L., McPartlin, J. M., Kirke, P. N., Lee, Y. J., Conley, M. R., Weir, D. G., and Scott, J. M. (1995) *Lancet 345*, 149−151.
10. O'Leary, V. B., Parle-McDermott, A., Molloy, A. M., Kirke, P. N., Johnson, Z., Conley, M., Scott, J. M., and Mills, J. L. (2002) *Am. J. Med. Genet. 15*, 107−111.
11. Porter, T., and Kasper, C. (1985) *Proc. Natl. Acad. Sci. U.S.A. 82*, 973−977.
12. Paine, M. J., Garner, A. P., Powell, D., Sibbald, J., Sales, M., Pratt, N., Smith, T., Tew, D. G., and Wolf, C. R. (2000) *J. Biol. Chem. 275*, 1471−1478.
13. Bredt, D. S., Hwang, P. M., Glatt, C. E., Lowenstein, C., Reed, R. R., and Snyder, S. H. (1991) *Nature 351*, 714−718.
14. Drennan, C. L., Huang, S., Drummond, J. T., Matthews, R. G., and Ludwig, M. L. (1994) *Science 266*, 1669−1674.
15. Wolthers, K. R., Basran, J., Munro, A. W., and Scrutton, N. S. (2003) *Biochemistry 42*, 3911−3920.
16. Shen, A. L., and Kasper, C. B. (2000) *J. Biol. Chem. 275*, 41087−41091.
17. Sheta, E. A., McMillian, K., and Masters, B. S. S. (1994) *J. Biol. Chem. 269*, 15147−15153.
18. Finn, R. D., Basran, J., Roitel, O., Wolf, C. R., Munro, A. W., Paine, M. J., and Scrutton, N. S. (2002) *Eur. J. Biochem. 270*, 1164−1170.
19. Gutierrez, A., Lian, L.-Y., Wolf, C. R., Scrutton, N. S., and Roberts, G. C. K. (2001) *Biochemistry 40*, 1964−1967.
20. Knight, K., and Scrutton, N. S. (2002) *Biochem. J. 367*, *19*−*30*.
21. Miller, R. T., Martasek, P., Omura, T., and Masters, B. S. S. (1999) *Biochem. Biophys. Res. Commun. 265*, 184−188.
22. Olteanu, H., Munson, T., and Banerjee, R. V. (2002) *Biochemistry 41*, 13378−13385.
23. Viola, R. E., Cook, P. F., and Cleland, W. W. (1979) *Anal. Biochem. 96*, 340−344.
24. Gutierrez, A., Doehr, O., Wolf, C. R., Scrutton, N. S., and Roberts, G. C. K. (2000) *Biochemistry 39*, 15990−15999.
25. Wang, M., Roberts, D. L., Paschke, R., Shea, T. M., Masters, B. S., and Kim, J. J. (1997) *Proc. Natl. Acad. Sci. U.S.A. 94*, 8411−8416.
26. Munro, A., Noble, M. A., Robledo, L., Daff, S. N., and Chapman, S. K. (2001) *Biochemistry 40*, 1956−1963.
27. Noble, M. A., Munro, A. W., Rivers, S. L., Robledo, L., Daff, S. N., Yellowlees, L. J., Shimizu, T., Sagami, I., Guillemette, J. G., and Chapman, S. K. (1999) *Biochemistry 38*, 16413−16418.
28. Gutierrez, A., Paine, M., Wolf, C., Scrutton, N. S., and Roberts, G. C. K. (2002) *Biochemistry 41*, 4626−4637.

BI0356303